Computational Mechanics 23 (1999) 144–150 © Springer-Verlag 1999

Parallel finite element method utilizing the mode splitting and sigma coordinate for shallow water flows

K. Kashiyama, Y. Ohba, T. Takagi, M. Behr, T. Tezduyar

Abstract Parallel finite element method for the analysis of quasi-three dimensional shallow water flow is presented. The mode splitting technique and the sigma coordinate (generalized coordinate) are employed to use parallel computers effectively. Parallel implementation of the unstructured grid-based formulation is carried out on the Hitachi parallel-super computer SR2201. The tidal flow of Tokyo Bay is simulated for a numerical example. The speed-up ratio and the efficiency of the parallelization are investigated. The present method is shown to be a useful and powerful tool for the large scale computation of shallow water flows.

1 Introduction

The shallow water flow analysis is usefully applied to the flows in oceans, lakes and rivers. A number of numerical methods for the shallow water flow based on the two dimensional model have been presented in the past. The present authors have been presented a parallel finite element method to solve the large scale computations of shallow water flows, such as the storm surges and tidal flows, using the fine mesh which represents the geography accurately (Kashiyama et al. (1995, 1997), Tezduyar et al. (1996)). However, in order to compute the sediment transport, the dispersion of contaminants, the exchange of sea water and so on accurately, it is necessary to evaluate the vertical velocity profile. Several quasi-three dimensional models have been also presented and these models are roughly classified into two approaches; the level model (Kawahara and Kobayashi (1983), Robert and Ouellet (1987)) and the sigma coordinate model (Sheng and Lick (1978), Sheng and Butler (1982), Takagi and Kawahara (1996)). In the level model, as the depth of each layer is assumed to be constant, the total number of layers is not to be constant over the whole domain due to the variation of water depth. From this, it is pointed out that the numerical accuracy in the bottom layer is worse. On the other hand, in the sigma coordinate model which introduce the generalized coordinate to the vertical direction, the total number of layer is to be constant over the whole domain. This approach can avoid the above mentioned disadvantage of the level model. Furthermore, it can be expected that this method is effective for the parallel computation, since the load balance can be easily equalized in each processor.

This paper presents a parallel finite element modeling utilizing the mode-splitting and sigma coordinate for the quasi-three dimensional shallow water analysis. The three dimensional flow field is divided into two fields; the horizontal flow field and the vertical flow field. The quasi-three dimensional flow analysis can be achieved by solving both field mutually. The finite element method is employed for the horizontal flow field and the finite difference method is employed for the vertical distribution of flow field. Parallel implementation of the unstructured-grid-based formulations are carried out on the Hitachi parallel-super computer SR2201. The effect of parallelization on the efficiency of the computations are examined.

2 Governing equations

The shallow water equations can be obtained from the conservation of momentum and mass, assuming a hydrostatic pressure distribution:

$$\dot{u}_i + u_j u_{i,j} + g\zeta_{,i} - (N_v u_{i,z})_{,z} - (N_h u_{i,j})_{,j} = 0 \qquad (1)$$

K. Kashiyama, Y. Ohba
Department of Civil Engineering, Chuo University,
1-13-27 Kasuga,
Bunkyo-ku, Tokyo 112-8551, Japan

T. Takagi
Coastal Engineering Department, INA Corporation,
1-44-10 Sekiguchi,
Bunkyo-ku, Tokyo 112-8668, Japan

M. Behr
Army HPCRC, University of Minnesota,
1100 Washington Avenue South,
Minneapolis, MN 55415, USA

T. Tezduyar
Mechanical Engineering and Material Science,
Army HPC Research Center, Rice University,
MS 321, 6100 Main Street,
Houston, TX 77005, USA

Correspondence to: K. Kashiyama

This research was supported by the grant-in-aid for encouragement of young scientist of the Ministry of Education, Science, Sports and Culture, No. 09750562. Partial support for this was also provided by the Army High Performance Computing Research Center under the auspices of the Department of the Army, Army Research Laboratory cooperative agreement number DAAH04-95-2-0003 and contract number DAAH04-95-C-0008. The content does not necessarily reflect the position or the policy of the Government, and no official endorsement should be inferred.

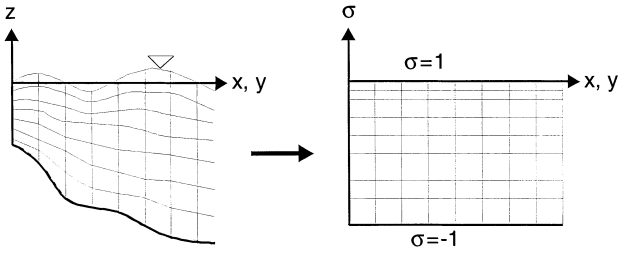

Fig. 1. Sigma coordinate

$$\dot{\zeta} + \left(\int_{-h}^{\zeta} u_i \, \mathrm{d}z \right)_{,i} = 0 \tag{2}$$

where u_i is the horizontal velocity, ζ is the water elevation, h is the water depth, g is the gravity acceleration, N_v is the vertical eddy viscosity coefficient and N_h is the horizontal eddy viscosity coefficient.

The following transformation form which is referred as the sigma coordinate is defined to introduce the generalized coordinate to the vertical direction (see Fig. 1).

$$\sigma = 1 - 2\frac{\zeta - z}{h + \zeta} = 1 - 2\frac{\zeta - z}{D} \tag{3}$$

where D is the total water depth. Introducing Eq. (3) into Eqs. (1) and (2), the governing equations can be expressed as follows.

$$\dot{u}_i + u_j u_{i,j} + \omega u_{i,\sigma} + g\zeta_{,i} - \frac{4}{D^2}(N_\mathrm{v} u_{i,\sigma})_{,\sigma} - (N_\mathrm{h} u_{i,j})_{,j} = 0 \tag{4}$$

$$\dot{\zeta} + (Du_i)_{,i} + (Dw)_{,\sigma} = 0 \tag{5}$$

in which

$$\omega(x_i, \sigma, t) = \frac{2}{D} w - \frac{\sigma + 1}{D}\dot{\zeta} - \frac{\gamma_i}{D} u_i \tag{6}$$

$$\gamma_i = \frac{1}{D}((\sigma - 1)h_{,i} + (\sigma + 1)\zeta_{,i}) \tag{7}$$

where w is the vertical velocity.

The velocity u_i can be assumed to be the sum of the depth averaged velocity and the variations around the averaged velocity as:

$$u_i(x_i, z, t) = U_i(x_i, t) + u_i'(x_i, z, t) \tag{8}$$

where U_i is the depth averaged velocity and u_i' is the variations around the averaged velocity. Integrating the Eqs. (4) and (5) over the depth and the wave phase using the above assumption (8), the following equations can be derived.

$$\dot{U}_i + U_j U_{i,j} + g\zeta_{,i} + \frac{1}{D}\left(\int_{-h}^{\zeta} u_i' u_j' \, \mathrm{d}z \right)_{,j} - \frac{1}{\rho D}(\tau_{si} - \tau_{bi}) - (N_\mathrm{h} U_{i,j})_{,j} = 0 \tag{9}$$

$$\dot{\zeta} + (DU_i)_{,i} = 0 \tag{10}$$

where τ_{si} and τ_{bi} denote the surface shear stress and the bottom shear stress respectively, which can be expressed as:

$$\tau_{si} = C^* \rho_a W_i |W| \tag{11}$$

$$\tau_{bi} = \frac{g}{C^2} \rho_w u_i^{(b)} |u^{(b)}| \tag{12}$$

where C^* is the surface friction coefficient, W is the wind velocity, $u_i^{(b)}$ is the velocity at the bottom, C is the Chezy's coefficient, ρ_a and ρ_w are the density of air and water, respectively. As the contribution of the fourth term of Eq. (9) is negligible small comparing with other terms, the term is ignored in the discretization.

3 Mode splitting method

A splitting algorithm for the external and internal modes is employed to study the three dimensional phenomena and to reduce the large amount of computational work. The governing equations for the external mode have been derived as Eqs. (9) and (10). The governing equations for the internal mode can be defined as the residual equation between Eqs. (4) and (9) as:

$$\dot{u}_i' + u_j u_{i,j} - U_j U_{i,j} + \frac{\partial \sigma}{\partial t} u_{i,\sigma}' - \frac{4}{D^2}(N_\mathrm{v} u_{i,\sigma})_{,\sigma} - (N_\mathrm{h} u_{i,j})_{,j} + \frac{1}{\rho D}(\tau_{si} - \tau_{bi}) - \frac{1}{D}\left(\int_{-h}^{\zeta} u_i' u_j' \, \mathrm{d}z \right)_{,j} = 0 \tag{13}$$

The stability condition of an external mode in the numerical computation is governed by the CLF condition. The internal mode allows a much longer time increment since it is related to the internal wave propagation. The computation are performed in two time steps, a short time increment is applied to the external mode described by the vertically integrated equations and much longer time increment is applied to the internal mode. In this paper, the computation of internal mode is performed at every 4

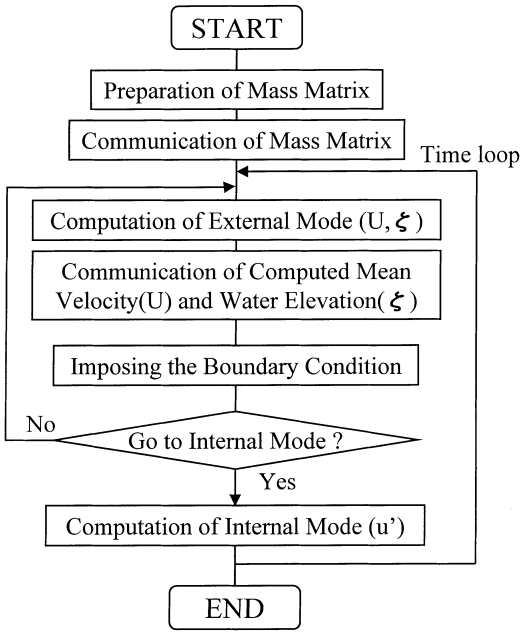

Fig. 2. Flow chart

steps of the external mode. Figure 2 shows the flow chart for the computation.

Expanding the velocity $u_i'(x_i, \sigma, t)$ in terms of the depth-dependent function $f_k(\sigma)$ and the coefficients $A_{ki}(x_i, t)$ varying with horizontal position and through time, gives

$$u_i'(x_i, z, t) = \sum_{k=1}^{M} A_{ki}(x_i, t) f_k(\sigma) \tag{14}$$

where M is the total number of modes. Introducing Eq. (14) into (13) and integrating it the over the depth, finally, the following equation can be derived as:

$$\dot{A_{ki}} + \frac{4}{D^2}\lambda_k A_{ki} = \left(\frac{\tau_{si}}{\rho D}(2-\alpha_k) + \frac{\tau_{bi}}{\rho D}(\alpha_k - 2f_k(-1)) + \frac{4}{D^2}(\beta_1 u_{si} - \beta_2 u_{bi} f_k(-1)) - \frac{4}{D^2} U_i \lambda_k \alpha_k - E_i \alpha_k\right)\phi_k \tag{15}$$

in which

$$E_i = u_j u_{i,j} - U_j U_{i,j} + \frac{\partial \sigma}{\partial t} u'_{i,\sigma} - (N_h u_{i,j})_{,j} - \frac{1}{D}\left(\int_{-h}^{\zeta} u_i' u_j' \, dz\right)_{,j} \tag{16}$$

where λ_k is the eigenvalue, β_1 and β_2 are the parameters related to the boundary conditions at the surface and the bottom, α_k and ϕ_k are the constants. The details of the derivation of Eq. (15) are described in the references (Sheng and Lick (1978), Sheng and Butler (1982), Takagi and Kawahara (1996)). The last term of Eq. (15) is ignored in the discretization.

4
Numerical discretization

For the discretization of the governing Eqs. (9) and (10) for the external mode, the standard Galerkin method is used. The weak form of the governing equations can then be written as:

$$\int_\Omega U_i^* \left(\dot{U}_i + U_j U_{i,j} + g\zeta_{,i} - \frac{1}{\rho D}(\tau_{si} - \tau_{bi})\right) d\Omega + \int_\Omega U_{i,j}^* (\bar{N}_h U_{i,j}) \, d\Omega - \int_\Gamma U_i^* t_i \, d\Gamma = 0 \tag{17}$$

$$\int_\Omega \zeta^* (\dot{\zeta} + (DU_i)_{,i}) \, d\Omega = 0 \tag{18}$$

where U^* and ζ^* denote the weighting functions and t_i represents the boundary term. Using the three-node linear triangular element for the spatial discretization, the following finite element equations can be obtained:

$$M_{\alpha\beta}\dot{U}_{\beta i} + K_{\alpha\beta\gamma j} U_{\beta j} U_{\gamma i} + H_{\alpha\beta i}\zeta_\beta + T_{\alpha\beta}\left(\frac{\tau_{ib}}{\rho D}\right)_\beta - T_{\alpha\beta}\left(\frac{\tau_{is}}{\rho D}\right)_\beta + S_{\alpha i\beta j} U_{\beta j} = 0 \tag{19}$$

$$M_{\alpha\beta}\dot{\zeta}_\beta + B_{\alpha\beta i\gamma} U_{\beta i} D_\gamma + C_{\alpha\beta\gamma i} U_{\beta i} D_\gamma = 0 \tag{20}$$

The bottom stress term is linearized and the water depth is interpolated using linear function.

For the discretization in time, the three-step explicit time-integration scheme is employed. The selective lumping technique is used for the numerical stabilization. The stability limit of this method is 1.5 times larger than that of the conventional two step scheme (Kawahara and Kashiyama (1984)). The details of this method is given in the reference (Kashiyama et al. (1995, 1997)). Applying this scheme to the finite element equations, the discretized equations in time can be obtained.

On the other hand, for the discretization of the governing Eq. (15) for the internal mode, the central difference scheme is employed as:

$$A_{ki}^{n+1} = \frac{1 - 2\Delta t \lambda_k / D^2}{1 + 2\Delta t \lambda_k / D^2} A_{ki}^n + \frac{\Delta t C_{ki}^n \phi_k}{1 + 2\Delta t \lambda_k / D^2} \tag{21}$$

where

$$C_{ki}^n = \frac{\tau_{si}}{\rho D}(2-\alpha_k) + \frac{\tau_{bi}}{\rho D}(\alpha_k - 2f_k(-1)) + \frac{4}{D^2}(\beta_1 u_{si} - \beta_2 u_{bi} f_k(-1)) - \frac{4}{D^2}\lambda_k U_i \alpha_k \tag{22}$$

Introducing the computed coefficients A_{ki}^{n+1} into Eq. (14), the velocity of the internal mode can be obtained.

5
Parallel implementation

A parallel implementation using the MPI suitable for unstructured grids has been designed for use on the Hitachi parallel-super computer SR2201 of the University of Tokyo. Figure 3 shows the configuration of a SR2201 system. The SR2201 system consists of 1024 RISC processors with the three dimensional crossbar network and the direct memory access. Each processor possesses the memory of 64–256 MByte. Using 1024 processors, the peak computational speed reaches 307 GFLOPS. To minimize the amount of interprocessor communication, the automatic

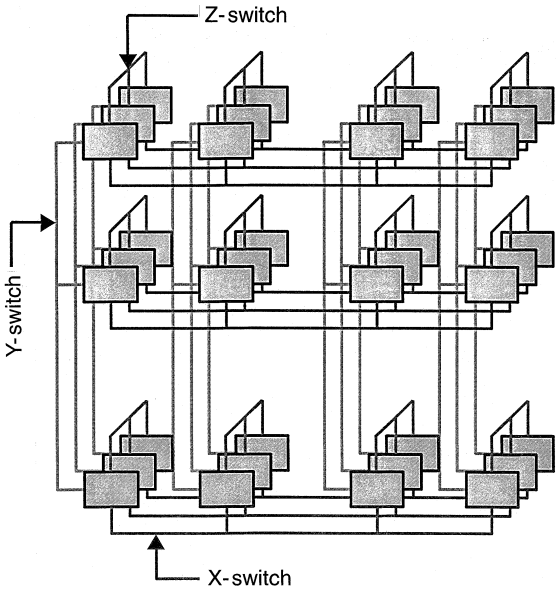

Fig. 3. SR2201 system

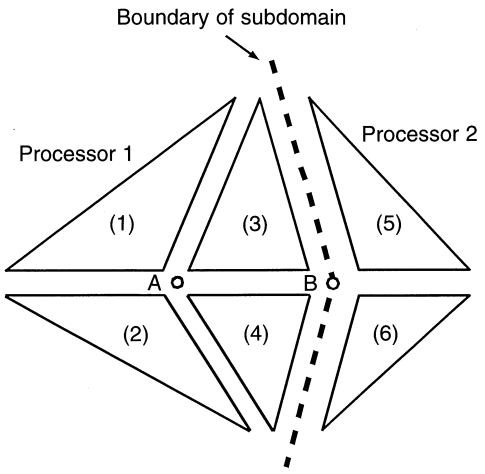

Fig. 4. Parallel implementation

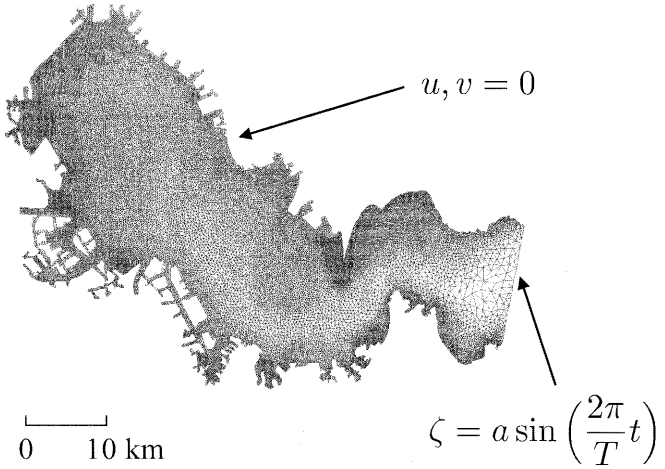

Fig. 5. Finite element idealization

mesh decomposer presented by Farhat (1988) is employed for the two dimensional plane mesh. For each subdomain, the processor associated with that subdomain carries out computations independently. No interprocessor communication is needed to compute the velocity of the internal mode because the fluctuated velocity can be locally determined on the vertical line at the nodal point of the horizontal finite element mesh.

The finite element equation for the external mode can be expressed as

$$\bar{\mathbf{M}}\mathbf{X} = \mathbf{F} \tag{23}$$

where $\bar{\mathbf{M}}$ is the lumped mass matrix, $\mathbf{X}$ is the unknown vector, $\mathbf{F}$ is the known vector. Figure 4 shows an example mesh with the bold line denoting the boundary of a subdomain. The elements (1)–(4) belong to the domain 1 (processor-1) and the elements (5) and (6) belong to the domain 2 (processor-2). The unknown values $\mathbf{X}$ are solved by:

$$\mathbf{X} = \mathbf{F}/\bar{\mathbf{M}} \tag{24}$$

No interprocessor communication is needed to compute the unknown values of the node which is located in the subdomain interior such as node A. However, in case of node B which is located on the boundary of subdomains, the interprocessor communication is needed and the procedure is described in the reference (Kashiyama et al. (1997)). The data transfer is performed at every time step (see Fig. 2). As the lumped mass matrix $\bar{\mathbf{M}}$ remains constant throughout the time step, the data transfer of that matrix is required only once.

6 Numerical example

As a numerical example, simulation of the tidal flow in Tokyo Bay is carried out. Figure 5 shows the finite element discretization. The total number of elements and nodes for external mode are 54 708 and 28 970, respectively. This mesh is designed to keep the element Courant number constant in the entire domain (Kashiyama and Okada (1992), Kashiyama and Sakuraba (1994)). It can be seen that an appropriate mesh accordance with the variation of water depth is realized. The total number of nodal points to the vertical direction is assumed to be 11. Therefore, the total number of nodes is to be 318 670. For the boundary

Fig. 6. Mesh partitioning for 256 processors

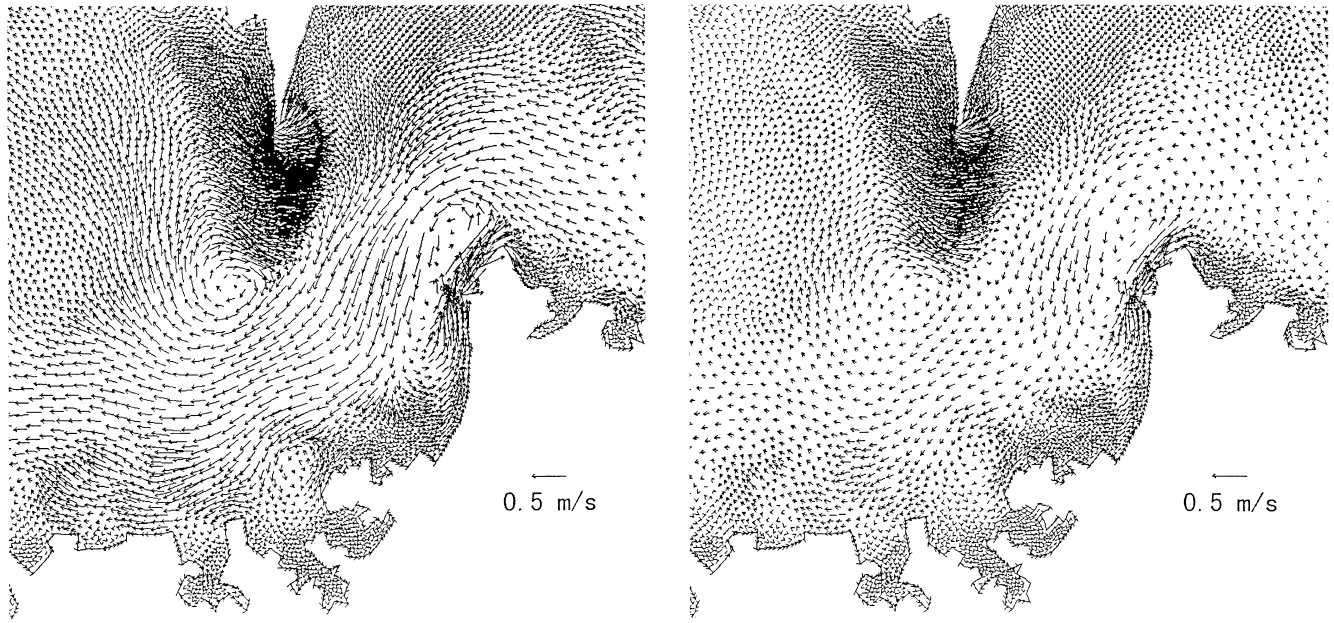

Fig. 7a, b. Computed current velocity at high tide at **a** surface layer and **b** bottom layer

condition, the non-slip boundary condition is applied to the coast line and the water elevation is specified at the open boundary. For the incident wave, the wave period is assumed to be 12.42 hours and the wave amplitude is assumed to be 0.36 m. The computation is started from the still water state. For the numerical condition, the following data are used; the Manning coefficients $n = 0.04$, the averaged horizontal eddy viscosity $\bar{N}_h = 10$ m^2/s, the vertical eddy viscosity coefficient $N_v = 0.001$, $\beta_1 = 0.0001$, $\beta_2 = 0.03$, the total number of modes $M = 30$. The time increments for the external mode and internal mode are assumed to be 3 second and 12 seconds, that is, the computation of internal mode is performed at every 4 steps of the external mode. Figure 6 shows the mesh partitioning for 256 processors. Figure 7 shows the computed current velocity at the high tide at the surface level (a) and the bottom level (b). Figure 8 shows the computed residual velocity at the surface level (a) and the bottom level (b). From this, the significant residual velocity can be seen at the surface level. Figure 9 shows the comparison of tidal ellipse between computed and observed results at the observation point. From this figure, it can be seen that the results obtained by

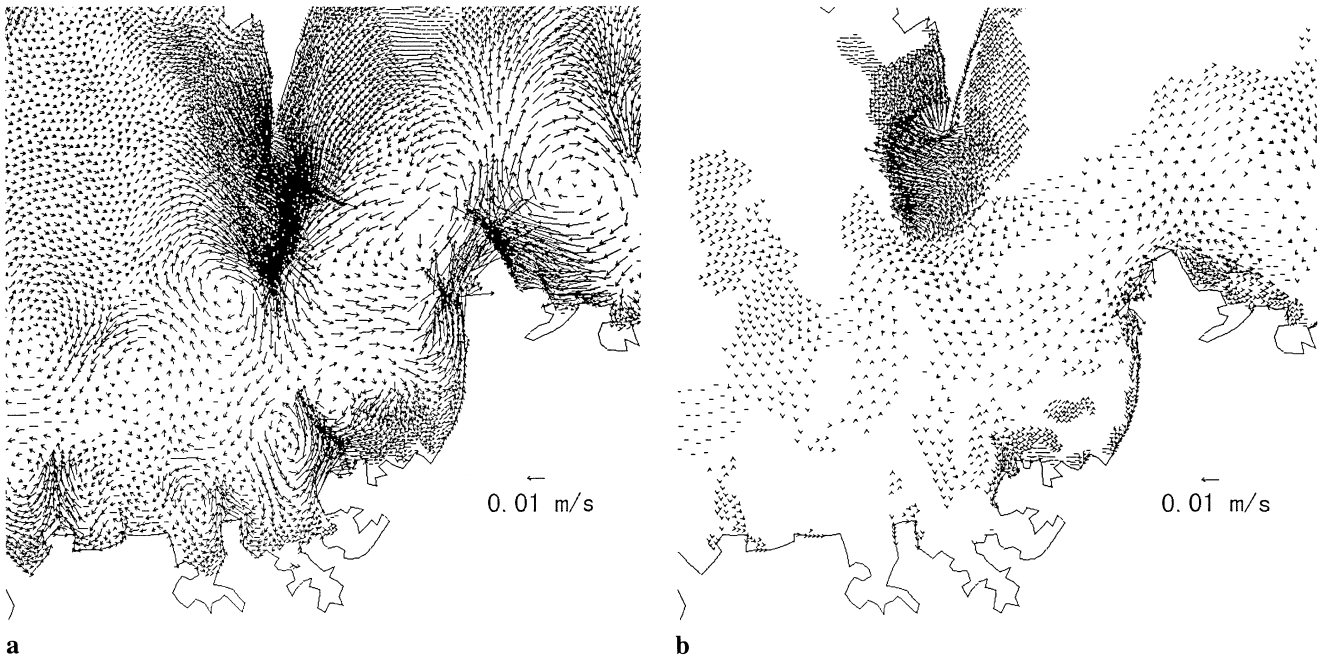

Fig. 8a, b. Computed residual current velocity at **a** surface layer and **b** bottom layer

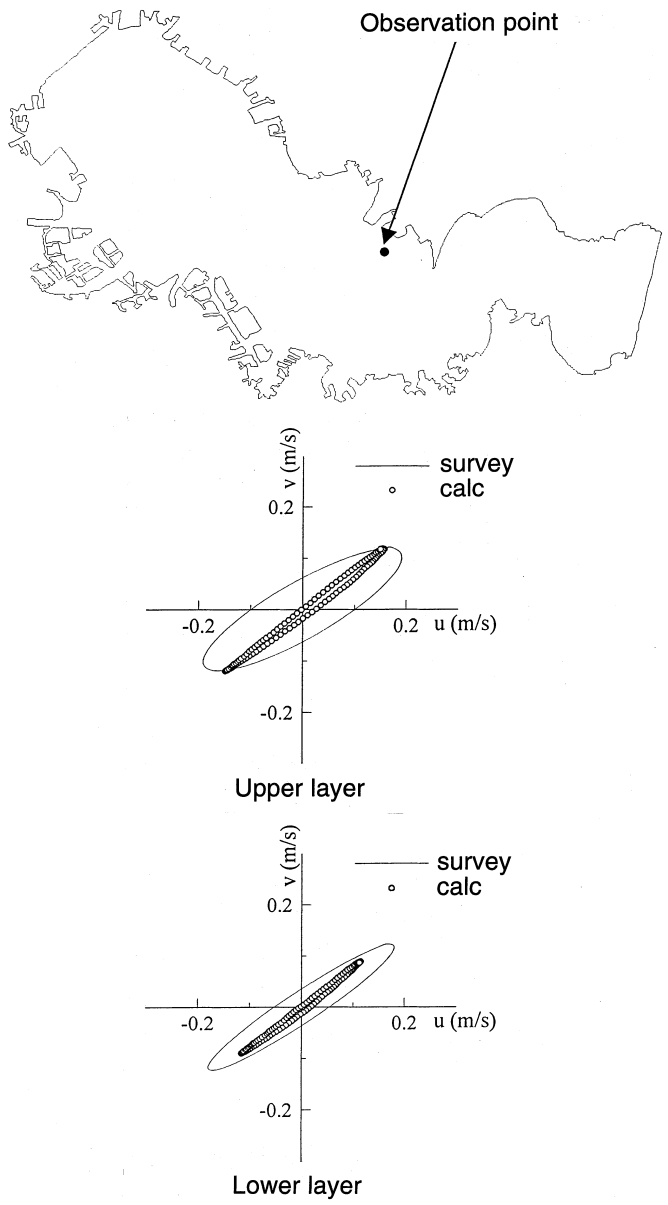

Fig. 9. Comparison of tidal ellipse between computed and observed results

the present method are reasonable agreement with observed data (Ministry of Transportation, 1983).

In order to check the performance of the parallelization, two types of finite element meshes are employed for external mode; mesh-*L*: 153 460 elements and 79 075 nodes, and mesh-*S*: 54 708 elements and 28 970 nodes. The total number of nodal points to the vertical direction is assumed to be 11. From this, the total number of nodes for mesh-*S* and mesh-*L* are to be 318 670 and 869 825 respectively. Figures 10 and 11 show the relation between the number of processors and speed-up ratio and the efficiency of parallelization respectively. In these figures, speed-up ratio and efficiency can be defined as:

$$\text{speedup ratio} = \frac{\text{computational time using 1 P.E}}{\text{computational time using } N \text{ P.E}} \tag{25}$$

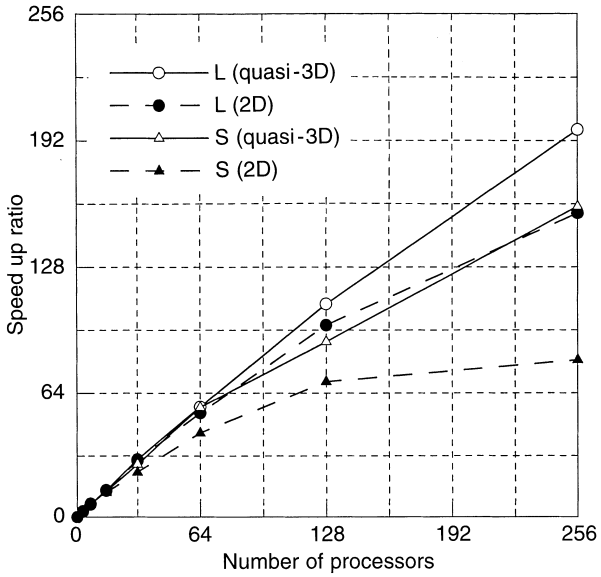

Fig. 10. Comparison of speed-up ratio

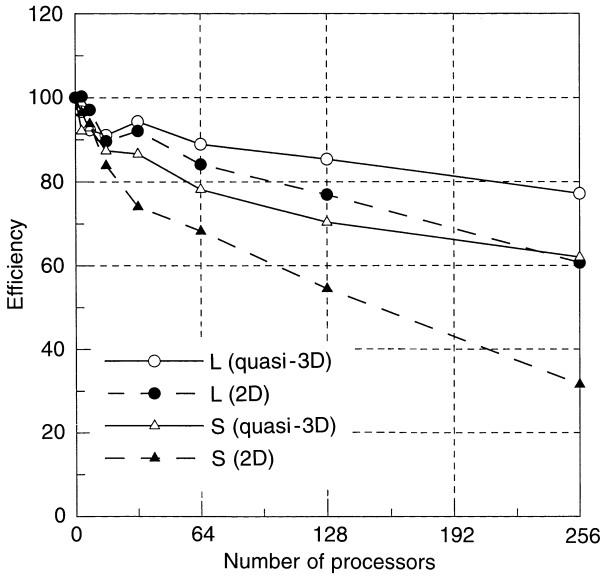

Fig. 11. Comparison of efficiency

Table 1. Details of CPU time

PE	2D		quasi-3D	
	pure CPU	com. & wait	pure CPU	com. & wait
1	74.25 (100.00%)	0.00 (0.00%)	681.239 (100.00%)	0.00 (0.00%)
8	8.92 (93.31%)	0.64 (6.69%)	88.69 (96.19%)	3.51 (3.81%)
64	1.12 (81.16%)	0.26 (18.84%)	11.30 (94.40%)	0.67 (5.60%)
128	0.49 (65.33%)	0.26 (34.67%)	5.70 (91.35%)	0.54 (8.65%)

(second, par 20 steps)

$$\text{efficiency} = \frac{\text{speedup ratio}}{N} \tag{26}$$

where N denotes the total number of processors. From these figures it can be seen that the performance is improved in accordance with the increase of the degree of freedom. Furthermore, the performance of the present method is greater than that of the two dimensional model. Table 1 shows the details of the CPU time for 20 time steps; the pure computational time, the waiting time and the communication time.

7 Conclusions

The parallel finite element method utilizing the mode-splitting and sigma coordinate has been presented for the analysis of quasi-three dimensional motion of shallow water flows. The method has been applied to the analysis of tidal flow in Tokyo Bay. The computed results have been compared with the observed data and the performance of parallelization has been investigated. The performance and efficiency were observed to improve linearly in accordance with an increase in the number of degree of freedom. From the results obtained in this paper, it can be concluded that the method is useful for the large scale computation of shallow water flows.

References

Farhat C (1988) A simple and efficient automatic FEM domain decomposer. Computers & Structures 28:576–602

Jiang CB, Kawahara M, Hatanaka K, Kashiyama K (1993) A three-step finite element method for convection dominated incompressible flow. Comp. Fluid Dyn. Journal 1:443–462

Kashiyama K, Okada T (1992) Automatic mesh generation method for shallow water flow analysis. Int. J. Number. Meth. Fluids 15:1037–1057

Kashiyama K, Sakuraba M (1994) Adaptive boundary-type finite element method for wave diffraction refraction in harbors. Comp. Meth. Appl. Mech. Eng. 112:185–197

Kashiyama K, Ito H, Behr M, Tezduyar TE (1995) Three-step explicit finite element computation of shallow water flows on a massively parallel computer. Int. J. Number. Meth. Fluids 21:885–900

Kashiyama K, Saitoh K, Behr M, Tezduyar TE (1997) Parallel finite element methods for large-scale computation of storm surges and tidal flows. Int. J. Number. Meth. Fluids 24:1371–1389

Kawahara M, Kobayashi M, Nakata K (1983) Multiple level finite element analysis and its applications to tidal current flow in Tokyo Bay. Appl. Math. Modelling 17:197–211

Kawahara M, Kashiyama K (1984) Selective lumping finite element method for nearshore current. Int. J. Numer. Methods Fluids 4:71–97

Ministry of Transportation (1983) Reports on the observation of tidal currents in Tokyo Bay. Port and Harbor Research Institute, Japan

Robert JL, Ouellet Y (1987) A three-dimensional finite element model for the study and non-steady natural flows, Three-Dimensional Models of Marine and Estuarine Dynamics Elsevier, 359–372

Sheng YP, Lick W, Gedney R, Molls F (1978) Numerical computation of the three-dimensional circulation in Lake Erie: a comparison of a free surface and a rigid-lid model, J. Phys. Oceano. 8:713–727

Sheng YP, Lee Butler H (1982) Modeling coastal currents and sediment transport, Proc. 18th Int. Conf. Coastal Eng. 1127–1148

Takagi T, Kawahara M (1996) Quasi-3 dimensional nearshore current simulation, FED-Vol. 238, Proc. 1996 Fluid Engineering Division Conference 3:457–461

Tezduyar TE, Aliabadi S, Behr M, Johnson A, Kalro V, Litke M (1996) Flow simulation and high performance computing. Computational Mechanics 18:397–412